

Hot-electron effects in metals

F. C. Wellstood,* C. Urbina,† and John Clarke

*Department of Physics, University of California, Berkeley, California 94720
and Materials Sciences Division, Lawrence Berkeley Laboratory, Berkeley, California 94720*

(Received 21 July 1993)

When sufficient electrical power P is dissipated in a thin metal film at millikelvin temperatures, the electrons can be driven far out of thermal equilibrium with the phonons. For uniform power dissipation in a volume Ω we show that the electrons attain a steady-state temperature $T_e = (P/\Sigma\Omega + T_p^5)^{1/5}$, where T_p is the phonon temperature and Σ is a parameter involving the electron-phonon coupling. We have used a sensitive ammeter based on a dc superconducting quantum interference device (SQUID) to measure the Nyquist current noise in thin films of AuCu as a function of P , and thus inferred T_e . We fitted our data to the theory with the single parameter Σ , and found good agreement for $\Sigma = (2.4 \pm 0.6) \times 10^9 \text{ Wm}^{-3} \text{ K}^{-5}$. When we increased the volume of the resistor by attaching a thin-film cooling fin, there was a much smaller increase in T_e for a given power dissipation in the resistor, in qualitative agreement with a simple model for nonuniform heating. We also measured the flux noise in dc SQUIDs at low temperatures, and found that the white noise was limited by heating of the electrons in the resistive shunts of the Josephson junctions. We were able to reduce these effects substantially by attaching cooling fins to the shunts.

I. INTRODUCTION

We can regard a thin metal film as a thermodynamic system which is composed of two interacting subsystems, the electrons and the phonons. If we suppose that the film is deposited on an insulating substrate, the phonon subsystem itself can be further subdivided into two parts: phonons in the metal and phonons in the substrate (see Fig. 1). The electron and phonon subsystems are coupled together by the electron-phonon interaction in the metal, and the two phonon subsystems are coupled together by energy flow across the interface between the film and the substrate. In our thermodynamic description, the electron-phonon interaction¹ produces a thermal resistance R_{ep} between the electrons and the phonons in the

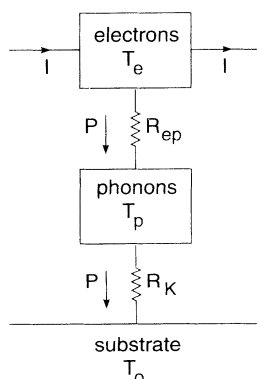


FIG. 1. Coupling between thermodynamic subsystems. Power P dissipated in the electron gas by current I flows into phonons via a thermal resistance R_{ep} mediated by the electron-phonon interaction and then into the electrically insulating substrate via a Kapitza resistance R_K .

metal while the interface between the film and the substrate produces a Kapitza boundary resistance R_K .² By attaching an external electrical supply to the metal we can apply power P to the electron system, causing its temperature to rise until it reaches a steady-state value such that power P is transferred to the phonons in the metal. Similarly, the temperature of the phonons in the metal increases until a power P is transferred to the substrate. If the electron-phonon coupling is weak, the electron and phonon subsystems attain well-defined, but different, steady-state temperatures.

At room temperature, the thermal resistance between the electrons and the phonons in a metal is exceedingly small, so that only very small temperature differences are generated at typical power levels. For example, the dissipation of 50 W in a 1 mm³ volume of Cu at 300 K would produce an electron-phonon temperature difference of only about 0.5 nK. Substantially larger temperature differences between the electrons and phonons would require so much power that the metal would be vaporized. Because of the strong effective coupling between the electrons and phonons, nonequilibrium effects in normal metals are generally of no significance at ordinary temperatures, except at very high power levels that can be produced, for example, by short intense laser pulses.³⁻⁷ On the other hand, at low temperatures—below say a few hundred millikelvin—the thermal resistance between the electrons and phonons is greatly increased, and it is possible to drive the electrons far out of thermal equilibrium with the phonons. This low-temperature regime is the subject of this paper.

In semiconductors, hot-electron effects at room temperature are well known.⁸ Because the carrier density is generally much smaller than in a metal, power is dissipated in a relatively small number of carriers and their temperature is correspondingly increased to a much greater

extent. The large carrier density of metals makes their hot-electron effects small at room temperature. At low temperatures, hot-electron effects in metals have been known for many years, since Little first estimated the magnitude of the effect.² The effect was first seen experimentally as a "hot-phonon effect" in experiments on heat exchangers for dilution refrigerators.⁹⁻¹¹ More recently, Arai established theoretically that an electron gas achieves a well-defined temperature when it is electrically heated and that this temperature could be found by measuring the Nyquist voltage noise.¹² Following Arai's work, Roukes *et al.*¹³ use a dc superconducting quantum interference device (SQUID) to measure the Nyquist noise in current-biased Cu films at low temperatures. They observed hot-electron effects in the films and interpreted their data in terms of a simple heating model based on an argument by Anderson, Abrahams, and Ramakrishnan.¹⁴ Subsequently, Wellstood and co-workers^{15,16} observed that the magnetic flux noise of dc SQUID's saturated as the temperature was lowered, and traced this effect to hot electrons in the thin-film AuCu alloy resistive shunts of the Josephson junctions. They also showed that the electron temperature could be significantly reduced by the addition of an appropriate cooling fin. Hot-electron effects have also been reported in weak-localization studies¹⁴ in thin films where they can contribute to the electron dephasing time.¹⁷

We note that hot-electron effects are particularly enhanced in thin films because the ratio of the power dissipated per unit volume to the power dissipated per unit area (that is, $1/d$, where d is the film thickness) can be made large. In addition, we expect the Kapitza resistance to be small for a very thin film at low temperatures, because the phonon distribution can no longer be considered to be separate from that in the substrate. To define a distinct population of phonons in a film of thickness d , we must be able to construct wave packets that include phonons with wavelengths at least as short as d . This implies a temperature $T \gtrsim \hbar v_s / 2k_B d$, where $v_s \approx 5 \times 10^3 \text{ ms}^{-1}$ is the velocity of sound. For a typical film thickness of 30 nm, we find $T \gtrsim 0.6 \text{ K}$. Thus, in the low-temperature regime below 0.1 K relevant to the present experiments, there is a negligible thermal phonon population with such short wavelengths. As a result, the phonon distribution becomes tied to that in the substrate and in this sense the usual Kapitza resistance becomes vanishingly small. In the low-temperature regime studied in this paper, the bottleneck in the transfer of heat from the electron gas in the film to the phonons in the substrate is provided by the weak electron-phonon interaction, rather than by a phonon Kapitza resistance at the film-substrate interface. In this regard, the heat transfer mechanism in our experiments is quite different from that studied in thicker films at higher temperatures.

From the above discussion, it is clear that hot-electron effects in metals are very closely related to the electron-phonon scattering rate. The literature on electron-phonon scattering in normal metals is extensive, and has been reviewed by Gantmakher.¹⁸ We note in particular the theoretical work of Nowak¹⁹ on bulk Cu and the theoretical and experimental work of Gantmakher and

Gasparov on bulk Cu and Ag.^{18,20,21} Except in the context of experiments on weak localization, there appears to have been relatively little work on electron-phonon scattering rates in disordered bulk metals or thin films.²²⁻²⁴

We begin, in Sec. II, with a theoretical analysis of hot-electron effects in normal metals, and derive an expression for the electron temperature in a small volume. In Secs. III and IV we describe our experiments to observe hot electrons in thin films at millikelvin temperatures, and in Sec. V present our results on dc SQUIDs. Section VI contains some concluding remarks.

II. THEORY OF THE HOT-ELECTRON EFFECT

A. Assumptions

To simplify our calculations of the magnitude of the hot-electron effect in a normal metal, we make the following assumptions.

(i) The electron gas is at a well-defined temperature $T_e \ll T_F$ which does not depend on position; T_F is the Fermi temperature. In our experiments, $T_e/T_F \leq 10^{-6}$. We note that Arai¹² has considered a nonthermal distribution of electrons, and concluded that a well-defined electron distribution does exist at low temperature and power. The assumption of a position-independent temperature implies uniform power dissipation.

(ii) The phonons are at a well-defined temperature $T_p \ll \theta_D$ which does not depend on position; θ_D is the Debye temperature. In our experiments, $T_p/\theta_D \leq 10^{-3}$. In this temperature limit, we can neglect optical phonons and need only consider acoustic phonons which, at low energies ϵ_q , have a linear dispersion relation $\epsilon_q = \hbar v_s q$, where \hbar is Planck's constant, v_s is the velocity of sound, and q is the phonon wave vector. Small departures from a thermal distribution result in only small corrections.¹⁶

(iii) The electrons have an isotropic, three-dimensional (3D) parabolic energy-band structure. Thus, the Fermi surface is spherical and an electron with wave vector \mathbf{k} has an energy $E_k = \hbar^2 k^2 / 2m^*$, where $k = |\mathbf{k}|$ and m^* is the effective mass of the electron.

(iv) The electron-phonon interaction is represented by a scalar deformation potential.¹ This assumption implies that only longitudinal phonons couple to the electrons so that we can neglect transverse phonons.

(v) Umklapp processes¹ can be neglected.

(vi) The dimensions of the metal are much longer than the average phonon wavelength. This assumption enables us to treat the allowed phonon states as a 3D continuum; we reconsider this assumption when we discuss thin films.

These assumptions enable us to derive a simple, exact expression for the electron temperature which clearly shows its dependence on the materials parameters of the metal. However, we need to consider the applicability of these assumptions to real materials such as the AuCu alloy used in our experiments. At millikelvin temperatures, the first two assumptions are well justified for virtually all metals. Assumption (iii) is a good approximation for alkali metals but can be a poor approximation for many

other metals. For example, in *pure* Au or Cu, the Fermi surfaces have necks which join together spheres in a multiple connected surface.²⁵ However, in an alloy these characteristic features are largely washed out by the short elastic lifetimes of the electrons. By the same token, (iv) is a poor assumption for pure Au or Cu because the scattering rate is known to vary strongly with position on the Fermi surface.¹⁹⁻²¹ This variation is predominantly due to the fact that transverse phonon modes can couple to the electrons in the neck regions.¹⁹ Such variations in the scattering should be averaged out in the alloy, leaving an isotropic interaction. However, even for the alloy, this assumption must be regarded only as an approximation, as more detailed analysis shows that coupling to transverse modes can arise.^{22,23} Similarly, (v) is not valid in pure Au or Cu because umklapp scattering occurs in the neck region even at very low temperatures.¹⁹ However, it is probably a better approximation in alloys, again because of the smearing of the Fermi surface. In any case, although umklapp processes are very important for momentum transfer because of the large change in wave vector, no such enhancement occurs in the energy transfer. Thus although our theoretical treatment could undoubtedly be refined, we believe it is an adequate approximation for our alloy samples.

B. Calculation of energy loss rate

The physical processes that transfer energy between the electron and phonon systems are shown in Fig. 2. An electron with wave vector \mathbf{k} and energy E_k emits or absorbs a phonon of wave vector \mathbf{q} and energy ε_q , changing its energy to $E_{k'}$ and wave vector to $\mathbf{k}' = \mathbf{k} \pm \mathbf{q}$. Since we have neglected umklapp processes, the wave vectors are strictly conserved. Using Fermi's golden rule, we write the rate at which an electron with wave vector \mathbf{k} is scattered to $\mathbf{k}' = \mathbf{k} - \mathbf{q}$ with the emission of a phonon as

$$\tau_{kk'}^{-1} = (2\pi/\hbar)M^2\delta(E_k - E_{k'} - \varepsilon_q)[1 - f(E_{k'})][n(q) + 1], \quad (2.1)$$

where $M^2 = (\hbar q / 2\rho v_s \Omega)(2\varepsilon_F/3)^2$ is the square of the matrix element for the deformation potential,¹ ρ and Ω are the mass density and volume of the metal, ε_F is the Fermi energy, $f(E_k)$ is the Fermi-Dirac distribution for the electrons, and $n(q)$ is the Bose-Einstein distribution for the phonons. The factor $(1-f)$ is the probability that the final electron state is empty and the factor $(n+1)$ accounts for the stimulated and spontaneous emission rate for the phonons. The rate at which the electron loses energy in this transition can be written as:

$$dU_{kk'}/dt = \varepsilon_q \tau_{kk'}^{-1}. \quad (2.2)$$

Summing over all allowed phonon wave vectors \mathbf{q} and all the initial electron states, we obtain the total rate at

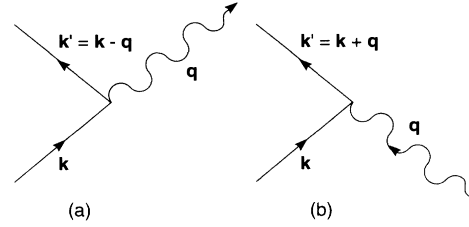


FIG. 2. Emission and absorption of phonons of wave vector \mathbf{q} by an electron of wave vector \mathbf{k} .

which the electron gas emits energy:

$$P_e = \frac{dU_{\mathbf{k}}}{dt} = \int f(E_{\mathbf{k}})D_e(\mathbf{k})d^3k \int \frac{dU_{\mathbf{k}\mathbf{k}'}}{dt} D_p(\mathbf{q})d^3q. \quad (2.3)$$

Here, $D_e(\mathbf{k})$ and $D_p(\mathbf{q})$ are the electron and phonon densities of states, respectively. Inspection of Eq. (2.3) reveals that the integrand depends only on the magnitude of \mathbf{k} ; for example, assumption (iv) implies that $D_e(\mathbf{k})$ depends only on \mathbf{k} . Accordingly, we can replace $D_e(\mathbf{k})d^3k$ by $D_e(E_k)dE_k$ where $D_e(E_k)$ is the electronic density of states with respect to energy. From Eqs. (2.1)–(2.3) we find

$$P_e = \int_0^\infty f(E_k)D_e(E_k)dE_k \times \int \frac{2\pi}{\hbar}M^2\varepsilon_q\delta(E_k - E_{k'} - \varepsilon_q) \times [1 - f(E_{k'})][n(q) + 1]D_p(\mathbf{q})d^3q. \quad (2.4)$$

A similar analysis for phonon absorption [Fig. 2(b)] yields the rate at which the electron gas absorbs energy from the phonons:

$$P_a = \int_0^\infty f(E_k)D_e(E_k)dE_k \times \int \frac{2\pi}{\hbar}M^2\varepsilon_q\delta(E_k - E_{k'} + \varepsilon_q) \times [1 - f(E_{k'})]n(q)D_p(\mathbf{q})d^3q. \quad (2.5)$$

The net rate P at which energy is transferred from the electrons to the phonons can thus be expressed as

$$P = P_e - P_a = P_0(T_e) - P_1(T_p), \quad (2.6)$$

where

$$P_0(T_e) = \int_0^\infty f(E_k)D_e(E_k)dE_k \times \int \frac{2\pi}{\hbar}M^2\varepsilon_q[1 - f(E_{k'})] \times \delta(E_k - E_{k'} - \varepsilon_q)D_p(\mathbf{q})d^3q \quad (2.7a)$$

and

$$P_1(T_p) = \int_0^\infty f(E_k)D_e(E_k)dE_k \int \frac{2\pi}{\hbar}M^2[1 - f(E_{k'})]\varepsilon_q \{ \delta(E_k - E_{k'} - \varepsilon_q) - \delta(E_k - E_{k'} + \varepsilon_q) \} n(q)D_p(\mathbf{q})d^3q. \quad (2.7b)$$

The term P_0 describes the rate at which the electron gas emits energy when the phonon gas is at zero temperature. The term P_1 describes the rate at which the phonons transfer energy to the electron gas when the electron gas is at zero temperature. While we see immediately from Eq. (2.7a) that P_0 does not depend on T_p , it is less obvious that P_1 is independent of T_e ; this fact can be demonstrated explicitly by evaluating Eq. (2.7b). Using assumptions (i)–(v) we can evaluate Eqs. (2.7a) and (2.7b) analytically to find

$$P_0 = \Sigma \Omega T_e^5 \quad (2.8a)$$

and

$$P_1 = \Sigma \Omega T_p^5, \quad (2.8b)$$

where

$$\Sigma = \frac{\hbar}{2\rho v_s} \left[\frac{2\varepsilon_F}{3} \right]^2 \frac{D(\varepsilon_F) k_B^5 \Gamma(5) \zeta(5)}{2\pi \hbar^5 v_s^3 v_F \Omega}.$$

Here, v_F is the Fermi velocity, $\Gamma(n) = (n-1)(n-2) \dots (1)$ is the gamma function, $\zeta(n)$ is the Riemann zeta function, and $\zeta(5) \approx 1.037$.

The expression for Σ can be simplified by noting that it contains factors involving the heat capacity of the electron gas and the average electron-phonon scattering rate. First, the electronic heat capacity per unit volume¹ is $C_{el} = \gamma T_e$, where

$$\gamma = \pi^2 D(\varepsilon_F) k_B^2 / 3\Omega. \quad (2.9)$$

Second, Ghantmakher¹⁸ has calculated the average electron-phonon scattering rate appropriate for our assumptions, and finds

$$1/\tau = \alpha^* T_e^3, \quad (2.10a)$$

where, rewriting his expression somewhat, we have

$$\alpha^* = \frac{6\zeta(3) k_B^3}{2\pi \mu \hbar^4 v_s^4 v_F} \left[\frac{2\varepsilon_F}{3} \right]^2. \quad (2.10b)$$

We can thus write

$$\Sigma = [6\zeta(5)/\pi^2 \zeta(3)] \alpha^* \gamma \approx 0.524 \alpha^* \gamma. \quad (2.11)$$

From Eqs. (2.8a) and (2.8b) we obtain the following simple expression for the net rate at which an electron gas in a metal transfers energy to the phonons:

$$P = \Sigma \Omega (T_e^5 - T_p^5). \quad (2.12)$$

When $T_e = T_p$, P vanishes, as it must when the electrons and phonons are in thermal equilibrium. The volume dependence arises from the fact that we calculated the rate for the entire gas, and the total number of electrons scales with Ω . It is interesting to compare our result with the Stefan-Boltzmann law for the exchange of electromagnetic radiation between two surfaces. In Eq. (2.12) the power scales as the difference of the fifth power of the temperatures and with the volume, whereas in the Stefan-Boltzmann law the power scales with the

difference of the fourth power of the temperatures and with the area.

Since in the steady state the power deposited in the electron gas by, for example, a current source must equal the power transferred to the phonon gas, Eq. (2.12) enables us to obtain T_e immediately:

$$T_e = \left[\frac{P}{\Sigma \Omega} + T_p^5 \right]^{1/5}. \quad (2.13)$$

Thus, the minimum temperature to which the electrons can cool, given by setting $T_p = 0$, is

$$T_{\min} = (P/\Sigma \Omega)^{1/5}. \quad (2.14)$$

We note that T_{\min} depends on the power per unit volume, and that this dependence is quite weak.

C. Criteria for observability

Now that we have established the magnitude of the hot-electron effect, we can discuss the conditions under which it should be observable. Clearly, we require that the electron temperature be significantly higher than the bath temperature. For hot-electron effects to be discernible, we also require that T_e be significantly higher than T_p . Accordingly, we adopt the following somewhat arbitrary set of criteria:

(i) $T_e \geq 2T_0$, where T_0 is the bath temperature.

(ii) $T_e - T_p > T_p - T_0$, that is, the temperature difference between the electrons and the phonons should exceed the temperature difference between the phonons and the bath, so that the increase in T_e is not predominantly due to thermal resistance between the phonon baths. Needless to say, somewhat different criteria could be adopted for (i) and (ii) depending upon the precision with which T_p , T_e , and T_0 can be measured. The above conditions are quite conservative, that is, if these conditions are satisfied the effect should be easy to see. We also require the consistency condition:

(iii) $T_e \geq T_p \geq T_0 \geq 0$.

If we consider a system with a fixed bath temperature T_0 , conditions (i)–(iii) define a region in the T_e, T_p plane where the hot-electron effect is observable [see Fig. 3(a)]. For a sample of a given size with a given bath temperature, there will be a definite functional relationship between T_e and T_p . We can find this relationship by noting that, in the steady state, the electrons transmit power to the phonons at the same rate as the phonons transmit power via a Kapitza resistance² to the heat bath. We can write

$$P = \Sigma \Omega (T_e^5 - T_p^5) = \sigma A (T_p^4 - T_0^4), \quad (2.15a)$$

where A is the contact area between the sample and the bath, $\sigma = 1/4R_K T_0^3$, and R_K is the Kapitza resistance of a unit area (in the limit of small temperature difference) between the sample and the bath. Rearranging this expression we can write:

$$T_e = T_p \left[1 + \frac{\sigma A}{\Sigma \Omega T_p} \left[1 - \frac{T_0^4}{T_p^4} \right] \right]^{1/5}. \quad (2.15b)$$

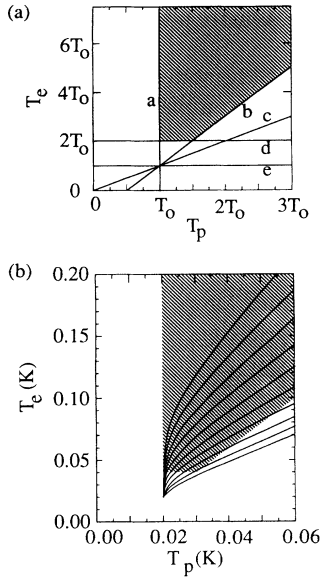


FIG. 3. (a) For fixed bath temperature T_0 , the shaded region is where the hot-electron effect is readily observable. Lines a–e are the relations $T_p = T_0$, $T_p - T_e = T_p - T_0$, $T_p = T_e$, $T_e = 2T_0$, and $T_e = T_0$, respectively. (b) Solid curves are the predicted T_e vs T_p for AuCu films of different thicknesses at a bath temperature of 20 mK. From top to bottom, the thicknesses are 3.75, 7.5, 15, 30, 60, 120, 240, 480, 960, and 1920 nm, respectively. The shaded area shows the region where the hot-electron effect is readily observable.

Different points along the curve $T_e(T_p)$ correspond to different applied power for the same bath temperature. If the curve passes through the region defined by conditions (i)–(iii) the hot-electron effect will be readily observable. Figure 3(b) shows the situation for films of different thicknesses at bath temperature $T_0 = 20$ mK, where we have used representative values of σ and Σ (see Sec. III). We see that for small film thickness, the $T_e(T_p)$ curve passes through the region of observability. However, as the thickness increases the temperature range over which the effect can be seen becomes smaller. The thickest film which still gives an observable effect is the one with a $T_e(T_p)$ curve which passes through the point $T_e = 2T_0$, $T_p = 1.5T_0$. Substituting this criterion into Eq. (2.15b) we find

$$T_0 = 0.166\sigma A / \Sigma \Omega. \quad (2.16)$$

If we assume the sample is a thin film of thickness d so that $\Omega = Ad$, Eq. (2.16) implies that the hot-electron effect will be readily observable provided that

$$T_0 \leq 0.166\sigma / \Sigma d. \quad (2.17)$$

We note that the film thickness is the only extensive parameter that enters into the observability, and we can expect to observe hot-electron effects at progressively higher bath temperatures by reducing d . For representative values of σ and Σ (see Sec. III) and our typical film thickness of 30 nm, Eq. (2.17) yields $T_0 < 0.74$ K; thus we expect the effects to be readily observable at temperatures

below 1 K. Decreasing the film thickness to 3 nm would increase T_0 by an order of magnitude, enabling one to observe these effects at liquid- ^4He temperatures.

D. Spatial dependence

In the above analysis, we have assumed that the temperature of the electron gas does not vary with position, as would be the case, for example, if we uniformly heated a thin film by passing a current through it. We now consider the effects of a nonuniform heating of the electron gas. The key concept to recognize is that at low temperatures the electrons travel a relatively large average distance, $l_{\text{in}} = v_F \tau$, before emitting a phonon; τ^{-1} is the phonon emission rate, which may be calculated from Eq. (2.10). At low temperatures in thin films, the inelastic scattering length l_{in} is much longer than the elastic mean free path, l_0 , so that electrons diffuse through the film making many elastic collisions before finally emitting a phonon. For example, for the AuCu alloy films discussed below we estimate $l_{\text{in}} \sim 10^4$ m and $l_0 \sim 10$ nm at 20 mK, yielding a diffusion length $l_d = (l_0 l_{\text{in}})^{1/2} \sim 10$ nm.

In general, nonuniform heating of the electron gas greatly complicates the calculation of heating effects. The essential difficulty is that the electron temperature need not be well defined. Different regions in the electron gas can exchange energy by exchanging electrons or via electron-electron collisions. At low temperatures, the electron-electron collision length can be relatively long, so that the electrons within a given small region are generally not in good thermal contact with each other and a well-defined temperature need not exist. We do not address this complication, but confine ourselves to a simplified model that is adequate for the present purpose. We consider a thin film in which heat is generated locally in some small region (Fig. 4) with dimensions very much less than l_d . The hot electrons diffuse out of this region over a mean distance l_d before they first emit a phonon. We assume that all the electrons in an effective area $A_{\text{eff}} = \pi l_d^2$ are at a uniform temperature T_e , and that $T_e \gg T_p$. In the steady state the power delivered from the electrons to the phonons is thus

$$P = \Sigma A_{\text{eff}} d T_e^5 = \Sigma \pi d l_0 v_F T_e^2 / \alpha^*, \quad (2.18)$$

where we have used Eq. (2.10a). Consequently, the electron temperature is given by

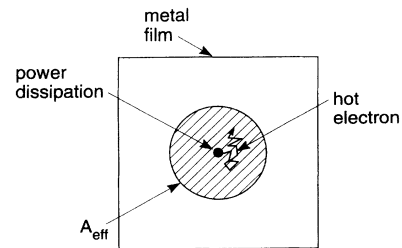


FIG. 4. Nonuniform-heating model. The power generated in a small region of film raises the electron temperature to T_e throughout the shaded area of radius l_d (electron diffusion length). Phonon emission occurs within the shaded area.

$$T_e = (P\alpha^* / \Sigma\pi dl_0 v_F)^{1/2}. \quad (2.19)$$

In this model T_e no longer scales as $P^{1/5}$ but rather as $P^{1/2}$. This scaling arises from the strong dependence of l_{in} on T_e ; as T_e increases l_{in} and thus the effective area A_{eff} decrease. Clearly for nonlocal heating T_e depends on the size, shape, and dimensionality of the sample—in this simple picture $P \sim T^{5-3N/2}$ for N dimensions. The calculations in Sec. II C correspond to the zero-dimensional case.

III. EXPERIMENTAL PROCEDURES

To investigate the hot-electron effect experimentally, it is necessary to address several issues: (i) the effect is most easily observable in a thin film at millikelvin temperatures, (ii) one must be able to measure T_p and T_0 or otherwise ensure that increases in T_e are not due to simple heating, and (iii) one must be able to measure T_e .

In view of (i) and (ii), we have designed our experiment so that we dissipate electrical power in a thin metal film deposited on a substrate immersed in liquid ^4He at millikelvin temperatures. At the relevant temperatures, the thermal phonon wavelengths are much larger than the film thickness, and so we expect the phonon temperature in the film to be the same as that in the substrate. Thus power P generated in the film raises the temperature of the substrate slightly above that of the surrounding ^4He bath, T_0 . We can estimate the temperature of the substrate from the Kapitza heating law in the form²

$$T_{sub} = (P/A\sigma + T_0^4)^{1/4}, \quad (3.1)$$

where A is the area of (both sides) of the substrate. Adopting the value²⁶ $\sigma = 20 \text{ W K}^{-4} \text{ m}^{-2}$ and taking $A = 50 \text{ mm}^2$ and $T_0 = 20 \text{ mK}$ we find the substrate temperature is raised by only 0.3 mK for a power dissipation of 10 pW. At higher bath temperatures, the temperature rise is even smaller at this power level. Thus, we shall approximate the phonon temperature of the film by T_0 ; as we shall see, the error so involved is negligible on the scale of the increase in the electron temperature.

We determined the electron temperature T_e by using the fact that the Nyquist noise produced by a resistive material scales with the temperature of the electrons.¹² At millikelvin temperatures, this noise is small and its measurement requires a very-low-noise amplifier, namely a dc SQUID. This technique has the advantage that the measurement of T_e is based directly on the fluctuation-dissipation theorem.

We performed experiments on two types of thin-film resistors. In the first, the hot electrons were confined to a relatively small volume in the vicinity of the region in which energy was dissipated. In the second, a thin-film “cooling fin” was attached to the resistor, allowing the hot electrons to diffuse into a much larger volume and reducing the temperature in the region in which dissipation occurred. We made electrical contact to the small normal-metal films by means of superconducting thin films. It is important to use superconducting wiring because normal contacts would introduce additional electrons which would cool the electrons in the resistor being

measured. In the superconducting state at temperatures well below the transition temperature, essentially all the electrons are paired and the electron thermal conductivity is vanishingly small. The electrons in the normal metal are prevented from penetrating into the superconducting film by Andreev reflection,²⁷ which reflects as holes any electrons with energies below the energy gap. Thus, the small normal-metal region cannot lose heat through electronic conduction to the leads and can cool only by emitting phonons.

A. Sample fabrication

The configurations of the two types of thin-film resistors, 1 and 2, are shown in Fig. 5. Resistor 1 [Fig. 5(a)] consists of a 36-nm-thick Au (25 wt %) Cu film evaporated on an oxidized silicon chip with an underlayer of 2.5 nm of Cr to ensure good adhesion. The films were lifted off to leave a $20 \times 30 \mu\text{m}^2$ rectangle. After cleaning the chip in detergent, we sputtered a 200-nm-thick film of Nb and patterned it with plasma etching to leave an approximately $2\text{-}\mu\text{m}$ -wide gap that defines the length of the AuCu resistor. The measured resistance between the Nb electrodes, 0.26Ω , was independent of temperature between 4.2 K and 20 mK and consistent with the resistivity and dimensions of the AuCu film. The lack of any temperature dependence strongly suggests that the proximity effect²⁸ between the Nb and AuCu films was negligible. At 20 mK, we estimate the pair decay length²⁸ in the AuCu, $\xi_N = (\hbar v_F l_0 / 6\pi k_B T)^{1/2}$, should be about $0.7 \mu\text{m}$ for an elastic electron mean free path l_0 of 20 nm. Since ξ_N is comparable with the length of the resistor, the lack of any temperature dependence of the resistance implies that the pair amplitude in the AuCu was extremely weak. There are two possible causes for the apparent lack of a proximity effect: first, apart from a degreasing step, we made no attempt to clean the surface of the AuCu before depositing the Nb, so that there was very likely a

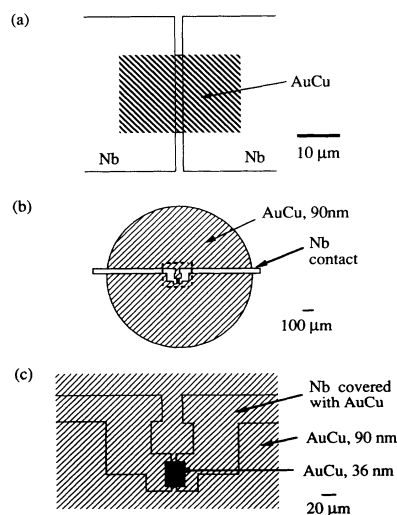


FIG. 5. Configuration of (a) small thin-film resistor, (b) large thin-film resistor; the dashed region in (b) is shown enlarged in (c).

thin layer of contamination or oxide between the two metals. This would weaken the diffusion of pairs into the metal, leading to a suppression of the pair wave function at the metal side of the interface. Second, the Cr underlayer was presumably at least partially oxidized to ferromagnetic Cr_2O_3 , providing a magnetic underlayer that would suppress superconductivity in the AuCu film. In our analysis of the data, although the dissipation occurs only in the 2- μm gap between the Nb electrodes, we assume that the hot electrons are distributed uniformly throughout the entire AuCu film.

Resistor 2 was fabricated with a large cooling fin in an attempt to reduce the temperature of the electrons in the volume in which dissipation occurred [see Figs. 5(b) and 5(c)]. To make this sample, we first deposited a 36-nm-thick AuCu film on an oxidized Si wafer and used photolithography and liftoff to pattern it into a $42 \times 30 \mu\text{m}^2$ rectangle. We then deposited and etched a 200-nm-thick Nb film to form 60- μm -wide contact electrodes which overlapped most of the rectangle, apart from a 7- μm gap. The sample was cleaned with an argon ion mill, and transferred to another vacuum chamber where a 90-nm-thick film of AuCu was deposited through a 1.4-nm-diam hole in a shadow mask centered on the gap between the Nb electrodes. As is evident from Fig. 5(c), the Nb contact lines had a somewhat complicated shape which allowed current to flow in an extended region around the 7- μm electrode gap. The measured resistance of the sample at low temperatures, 0.076 Ω , was reasonable consistent with that expected from the total thickness of AuCu between the ends of the Nb electrodes.

B. Measurement configuration

The measurement configuration^{15,16} is shown in Fig. 6. A square-washer dc SQUID was flux modulated at 500 kHz and operated in a conventional flux-locked loop in which the magnetic flux in the SQUID was maintained at a constant value.²⁹ The 20-turn input coil of the SQUID had a self-inductance L_i of about 120 nH and a mutual inductance M_i to the SQUID of about 6 nH. The input coil was coupled to a bias resistance R_0 of 0.072 Ω , the thin-film sample of resistance R (0.26 or 0.076 Ω), and a wire-wound superconducting inductor L_0 of about 10 μH . The purpose of the inductor was to prevent high-frequency signals and noise from the SQUID from reach-

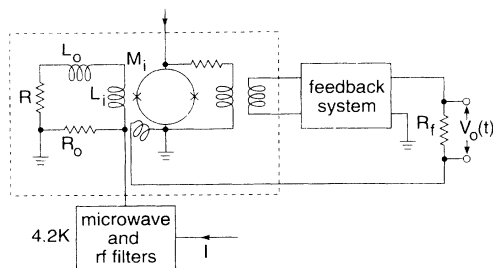


FIG. 6. Feedback circuit for measuring noise in resistor R . Components within the dashed line are cooled by a dilution refrigerator.

ing the sample; the roll-off frequencies for the high and low values of R were about 5 and 2 kHz, respectively. The resistor R_0 consisted of a 10-mm length of 100- μm -diameter Manganin wire. The resistor R_0 allowed us to apply bias voltage to the sample R , while providing a low-impedance path for noise currents generated by R to flow through the input coil L_i .

The low-temperature part of the experiment, enclosed in the dashed box in Fig. 6, was mounted in the experimental cell shown in Fig. 7. The sample and SQUID were attached to insulating supports which were bolted to a mount machined from a solid Nb rod. To shield against external magnetic interference, the mount was enclosed in a Nb tube which was open at one end. The tube was mounted rigidly in a Teflon sleeve that was surrounded in turn by an oxygen-free high-conductivity (OFHC) Cu can bolted to a stainless-steel flange with an In O-ring vacuum seal. Wires were brought out to a vacuum-tight electrical connector. Not shown in Fig. 7 is a capillary which was used to fill the cell with liquid ^4He , thereby ensuring that the interior was cooled. The top of the Cu can was attached via a screw thread to the mixing chamber of a dilution refrigerator and maintained good thermal contact. The temperatures of the mixing chamber and Cu can were measured with a combination of carbon and germanium thermometers.

The vacuum circuit components were attached to fiberglass or phenolic mounts that fitted rigidly into the Nb cell. The thin-film resistor was contained in the upper compartment (see Fig. 7), and the inductor L_0 in the compartment below. The SQUID and R_0 were in the next compartment, just above the output transformer. Wires between compartments were run in narrow channels. Thus each segment of the circuit was magnetically isolated from the others, and the entire cell provided a high degree of electrical and magnetic isolation from environmental noise. The current for the sample was provided by a battery-powered supply and was passed through low-pass 4.2-K microwave and radiofrequency filters to prevent high-frequency electrical power from reaching the sample. The dilution refrigerator was en-

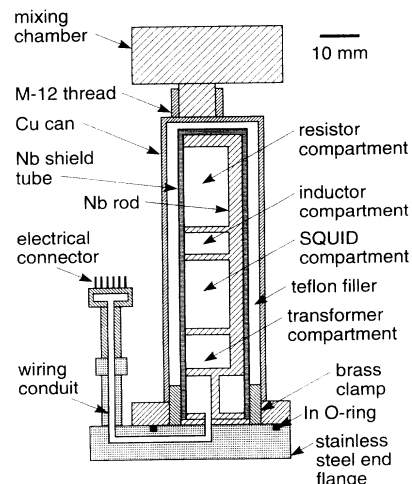


FIG. 7. Experimental cell.

closed in a screened room and the Dewar surrounded by a concentric μ -metal shield that reduced the ambient magnetic field to below $1 \mu\text{T}$.

The measurement procedure was as follows. We first filled the cell with liquid helium and stabilized the temperature of the mixing chamber at a predetermined value. We then biased the SQUID, applied a fixed level of current to the input resistor, and locked the feedback loop. The output $V_0(t)$ of the SQUID feedback electronics is proportional to the flux coupled into the SQUID. Since any current which flows through the sample must also flow through L_i and produce a flux in the SQUID, the feedback-loop output is also proportional to the current flowing through the sample resistor. The output from the feedback electronics was amplified and coupled into a spectrum analyzer, giving us a spectrum of the flux noise in the SQUID, or, equivalently, the current noise flowing through L_i . We obtained noise spectra by averaging the spectra from 256 individual time records, and stored the resulting data on a personal computer for later analysis.

C. Data analysis

The spectral density of the flux noise was measured from 1 Hz to 25 kHz. In our analysis, we excluded data below 10 Hz because the low-frequency noise from the SQUID became nonnegligible, and we excluded frequencies above 15 kHz because the noise and gain of the feedback loop began to differ from the low-frequency value. The spectra usually exhibited sharp lines due to microphonics and pickup of 60 Hz and its harmonics; data from frequencies in the neighborhood of these lines were also excluded from the analysis. The remaining spectrum contained contributions from four sources:

(i) The SQUID and its readout electronics, which had a flux-noise power spectrum of the form $S_0(f) + A(T)/f^{2/3}$. Here, $S_0(f)$ is the white noise of the electronics, and the second term describes the low-frequency flux noise of the SQUID,³⁰ which was measured in separate experiments. Typically, at $f=1$ Hz and at low temperatures, $S_0(f) \approx 6\mu\Phi_0 \text{ Hz}^{-1/2}$, whereas $A(T)/f^{2/3} = 9\mu\Phi_0 \text{ Hz}^{-1/2}$, so that the $1/f^{2/3}$ noise from the SQUID made a relatively small contribution to the amplifier noise above a few Hz.

(ii) Noise produced by Nyquist current noise from R at temperature T_e .

(iii) Noise produced by Nyquist current noise from R_0 at temperature T_0 (see discussion below).

(iv) Noise from the current supply used to bias the sample, which was white over the measured frequency range and of known current-noise power spectral density $S_1(f)$. This term was typically 10% or less of the total noise power.

The last three current-noise sources produced a Lorentzian flux-noise power spectrum in the SQUID with a knee frequency $f_k = (R + R_0)/2\pi(L_i + L_0)$. Thus the flux noise from all four sources has a spectral density of the form

$$S_\Phi(f) = S_0(f) + \frac{A(T)}{f^{2/3}} + \frac{M_i^2[S_R(f) + \eta^2 S_1(f)]}{1 + (f/f_k)^2}, \quad (3.2)$$

where M_i is the mutual inductance between the SQUID and the input coil, η is a known coupling coefficient which determines the fraction of the bias current which passes through R rather than R_0 , and $S_R(f)$ is the spectral density of the Nyquist current noise from R and R_0 . Once we had measured $S_\Phi(f)$, we analyzed the resulting data by varying $S_0(f)$, $M_i^2(S_R + \eta^2 S_1)$ and f_k to produce the best χ^2 fit. We then subtracted the known value of $M_i^2 \eta^2 S_1$ to leave $S_R(f)$. The fitting procedure yields estimates of $S_R(f)$ accurate to about $\pm 1\%$. The fit for f_k is accurate to about $\pm 10\%$, but fortunately errors in f_k produce only second-order errors in the estimate of $S_R(f)$. At low temperatures and with no power dissipated in R and R_0 , the white noise from the SQUID is comparable to the Nyquist noise in R and R_x , while the $1/f^{2/3}$ noise is comparable at about 3 Hz. At the higher levels of dissipation in the input circuit, the SQUID noise becomes negligible.

Our analysis yields the Nyquist noise from R and R_0 , and to proceed further we have to know the electron temperature of the latter. By choosing the volume of the Manganin wire to be large ($8 \times 10^{-11} \text{ m}^3$), we make the electron temperature very close to the phonon temperature: taking the value $\Sigma \approx 2 \times 10^9 \text{ W m}^{-3} \text{ K}^{-5}$ found by Roukes *et al.*¹³ for pure Cu, a power dissipation of 10 pW, and $T_p = 20$ mK, we find from Eq. (2.13) $T_e - T_p < 0.1$ mK. Furthermore, the surface area of the Manganin is sufficiently large, about 3 mm^2 , that the phonon temperature is close to the bath temperature. Under the conservative assumption that the Manganin loses energy only to the ^4He bath, from Eq. (3.1) at a power dissipation of 10 pW we find $T_p - T_0 < 4$ mK. As we shall see, this increase in the phonon temperature is very small compared to the increase in the electron temperature of the thin films at comparable power levels, and for simplicity we set $T_p = T_0$. Thus, in our analysis, we make the approximation that the electrons in R_0 are at temperature T_0 .

Under this assumption, the Nyquist noise current in the input circuit in the white-noise region $f < f_k$ has the following spectral densities for no power and power P dissipated in R :

$$S_R^{(0)}(f) = 4k_B T_0 / (R + R_0) \quad (P=0), \quad (3.3)$$

and

$$S_R^{(p)}(f) = 4k_B (T_e R + T_0 R_0) / (R + R_0)^2 \quad (P \neq 0). \quad (3.4)$$

Solving for T_e we find

$$T_e = T_0 \left[\frac{S_R^{(p)}(f)}{S_R^{(0)}(f)} \left(1 + \frac{R_0}{R} \right) - \frac{R_0}{R} \right]. \quad (3.5)$$

Given the measured values of T_0 , R , and R_0 , we use $S_R^{(0)}(f)$ as a check on the overall calibration of the system. We determine the ratio R_0/R by measuring the fraction of the current I that flows through the input coil of the SQUID (see Fig. 5). Thus, our measurement of T_e

involves a knowledge of T_0 and the ratios $S_R^{(p)}(f)/S_R^{(0)}(f)$ and R_0/R .

The power dissipated in R is given by

$$P = I^2(R_0^2 R)/(R + R_0)^2. \quad (3.6)$$

IV. RESULTS AND DISCUSSION FOR THIN FILMS

A. Resistor 1

Figure 8 shows the measured electron temperature T_e vs power dissipated at bath temperatures of 25 and 105 mK. At the lower bath temperature, we see that T_e is equal to the bath temperature for low levels of dissipation, crossing over to a power-law behavior at about 10^{-3} pW. At a bath temperature of 105 mK, the onset of observable heating effects is delayed to a higher power, about 0.1 pW, above which T_e tends asymptotically to the data for the lower bath temperature. This behavior is as expected from Eq. (2.13), which implies that $T_e = (P/\Sigma\Omega)^{1/5}$ for $T_e \gg T_p$.

The electron temperature can be fitted to a power law of the form

$$T_e = (P/\Sigma\Omega + T_0^n)^{1/n}. \quad (4.1)$$

The solid curve in Fig. 8 shows a χ^2 fit to the data at the 25-mK bath temperature. We note that the prediction for T_e mimics the abrupt crossover in the data from T_0 to the hot-electron regime. The fit is good and yields $\Sigma = (2.4 \pm 0.6) \times 10^9 \text{ W m}^{-3} \text{ K}^{-5}$ and $n = 4.87 \pm 0.05$. The uncertainty in the value of Σ is dominated by the uncertainty in T_0 : an error of $\delta\%$ in T_0 translates into an error of $5\delta\%$ in Σ . The value of n is about $2\frac{1}{2}$ standard deviations from the value of 5 predicted in Sec. II and is thus reasonably consistent with the hot-electron theory. One can rule out the value 4 that would result from a theory in which the electrons and phonons are at the same temperature and the phonon escape is limited by Kapitza resistance. To confirm the failure of the simple heating model, in Fig. 8 we have also plotted the result of

calculating T_e assuming that the electrons and phonons are at the same temperature and the phonons escape to the substrate via a Kapitza resistance [Eq. (3.1)]. The resulting dashed line has a slope at high power levels corresponding to $n=4$. We see that the crossover from $T_e = T_0$ to the heating regime occurs at about 10^{-1} pW, about two orders of magnitude above the observed crossover power. The large discrepancies between the data and the predictions in both the crossover power and the slope above this region argue strongly against the validity of the simple Kapitza heating model.

Our value of Σ is close to the value we infer from the work of Roukes *et al.*¹³ on Cu films, $1.8 \times 10^9 \text{ W m}^{-3} \text{ K}^{-5}$. By comparison, from the results of Anderson and Peterson¹¹ on bulk Cu, we infer $\Sigma = 1.0 \times 10^9 \text{ W m}^{-3} \text{ K}^{-5}$. From the electron-phonon scattering rate measurements of Gantmakher and Gasparov on pure Cu,²⁰ we can infer values of Σ ranging from $(0.1-1.1) \times 10^9 \text{ W m}^{-3} \text{ K}^{-5}$, where the higher rates are at the necks of the Fermi surface. Using the simple model presented in Sec. II, from Eqs. (2.10b) and (2.11) we predict that $\Sigma \approx 10^8 \text{ W m}^{-3} \text{ K}^{-5}$ for Cu, Ag, or Au. The fact that our model calculation for Σ is lower than most of the experimental results is possibly due to our assumption of a free-electron model and our neglect of the transverse phonon modes. The inclusion of both effects could significantly increase the electron-scattering rate and hence Σ .

B. Resistor 2

The purpose of this experiment was to investigate the effects of a large thin-film cooling fin attached to the small resistor in which power was being dissipated. In this situation, because the dimensions of the resistor are much less than l_d , hot electrons diffuse into the fin and virtually all the power transfer occurs in the large fins. This configuration is thus close to that considered in our effective-area model in Sec. II D. The measured values of T_e are plotted vs power in Fig. 9 for bath temperatures of 25 mK together with the values for resistor 1. We see

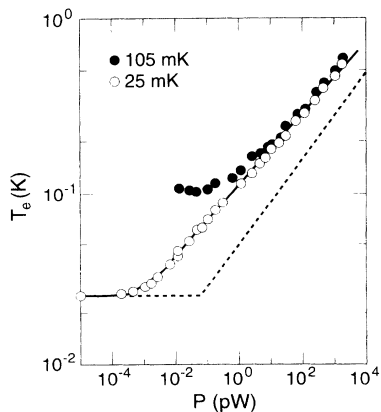


FIG. 8. Measured electron temperature T_e vs dissipated power for resistor 1 at two bath temperatures. The solid line is the fit of Eq. (4.1) to 25-mK data with $n = 4.87$. The dashed line is the “simple heating model.”

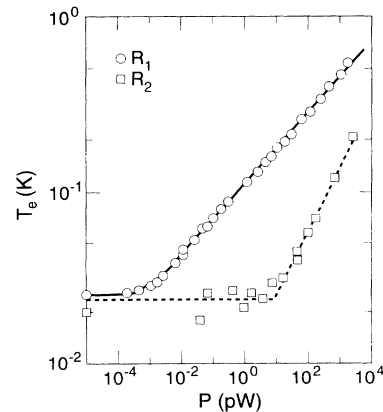


FIG. 9. Measured electron temperature T_e vs dissipated power for resistors 1 and 2 at bath temperature of 25 mK. The solid line is the fit of Eq. (4.1); the dashed line is to guide the eye.

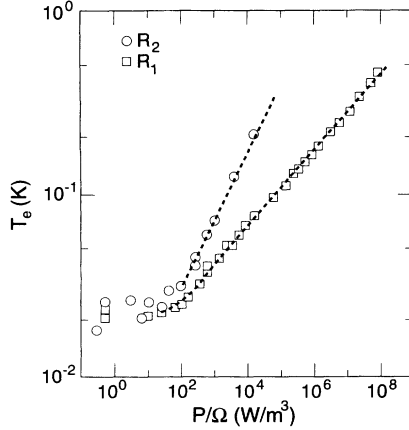


FIG. 10. Measured electron temperature T_e vs power per unit volume for resistors R_1 and R_2 at 25 mK. Dashed lines are guides to the eye.

that the cooling effect of the fin is enormous: compared to resistor 1 at 25 mK, resistor 2 must dissipate almost five orders of power more to increase T_e measurably above the bath temperature. Moreover, the slope for resistor 2 in the heating regime is markedly different, corresponding to $n=2.7$. Although this power is higher than the value of 2 given by our model in Sec. II, given the crudeness of the model this discrepancy is perhaps not surprising. The value of 2.7 is obviously much less than the value of 5 given by the uniform-heating model in Sec. II B and the value of 4 given by the picture in which electrons and phonons are at the same temperature and the phonons escape to the substrate via a Kapitza resistance.

We make a further comparison of the two resistors in Fig. 10, where we plot T_e vs P/Ω . In each case, we have used a value for Ω corresponding to the entire volume of AuCu film. We see that the value of P/Ω at which significant heating sets in, about 30 W m^{-3} , is roughly the same in both cases. This result is expected if we assume that both resistors are in the zero-dimensional limit (Sec. II B). Since we estimate the electron inelastic mean free path l_{in} to be about 5 nm at 25 mK, this assumption is reasonable. However, as the power and thus the temperature increase, l_{in} decreases and the *effective* area of the cooling fin of resistor 2 is reduced. As a result, T_e increases more rapidly for resistor 2 than for resistor 1 as the dissipation increases.

This result for resistor 2 demonstrates the dramatic effect the cooling-fin volume has in reducing the electron temperature for a given power dissipation. In Sec. V, we apply this result to a dc SQUID to reduce the effective electron temperature of the shunt resistors.

V. HOT-ELECTRON EFFECTS IN dc SQUIDS

The intrinsic white-noise energy sensitivity of the dc SQUID²⁹ is given by $\epsilon_v(f) = S_\Phi(f)/2L$, where $S_\Phi(f)$ is the spectral density of the flux noise in the SQUID and L is the inductance of the SQUID loop. The energy sensitivity characterizes the performance of the SQUID as a

small-signal amplifier, smaller values of ϵ_v corresponding to a more sensitive amplifier. For our SQUIDS, and most other low- T_c SQUIDS, the white flux noise originates from Nyquist noise in the normal-metal film resistors connected across the Josephson tunnel junctions to eliminate hysteresis from the current-voltage (I - V) characteristic. The SQUID is a nonlinear device, and the voltage noise across it at frequencies well below the Josephson frequency f_J is greater than the Nyquist value, because additional noise is mixed down from frequencies near f_J . Numerical simulations predict^{29,31,32}

$$\epsilon_v(f) = (9 \pm 1) k_B T L / R \quad (5.1)$$

for $\beta_L = 2LI_0/\Phi_0 = 1$ and $\beta_c = 2\pi I_0 R^2 C / \Phi_0 < 1$ (I_0 , R , and C are the critical current, shunt resistance, and capacitance of each junction, and $\Phi_0 = h/2e$ is the flux quantum). Since the noise is produced by Nyquist noise in the resistive shunts, it is clear that the temperature T should be replaced by T_e , the temperature of the electrons in the shunts. Thus, in the thermal limit, one expects $\epsilon_v(f)$ to scale with T_e . If T_e , L , and C are reduced sufficiently, quantum effects should take over and the noise energy is expected to flatten off at a value³³ of approximately \hbar . However, much of the current biasing the SQUID flows through the shunt resistances, and, as one reduces the temperature into the millikelvin range, hot-electron effects become increasingly important. Thus the noise energy may well flatten out at a value substantially above \hbar , the quantum limit. In this section we demonstrate such effects in SQUIDS, and show that they can be significantly reduced by attaching cooling fins to the shunts.

A. Experimental procedures

All of the SQUIDS (shown in Fig. 11) were fabricated on oxidized Si wafers and had Au (25 wt %) Cu resistive shunts with a 2.5-nm Cr underlayer 200-nm thick. After patterning the shunts, we deposited and patterned Nb base electrodes which were covered with a 400-nm layer of SiO in which two $2 \times 2\text{-}\mu\text{m}^2$ windows were opened to form the tunnel junctions. After using an Ar (5 vol %) O_2 plasma to grow a native oxide barrier on the Nb, we evaporated a 200- μm -thick Pb (5 wt %) In counterelectrode to complete the Josephson tunnel junctions. The estimated inductance of the SQUID loop was 0.5 nH, and the shunt resistance of each junction was 6 Ω .

In the case of SQUIDS D_1 and D_2 [Fig. 11(a)], the AuCu shunts were 30-nm thick with combined area and volume listed in Table I. For SQUID M_1 each shunt was extended to form a large, $400 \times 400\text{-}\mu\text{m}^2$ cooling fin [Fig. 11(b)]. In the case of M_2 , we increased the volume of these fins by depositing and lifting off an additional 900 nm of CuAu while leaving the shunt thickness at 30 nm. Each fin was covered with about 400 nm of SiO followed by about 200 nm of PbIn. The purpose of the PbIn was to screen Nyquist noise currents in the fins that, particularly in the case of the thicker fins, might produce a significant flux noise in the SQUID. The total volume and area of AuCu are listed in Table I. Thus, the volume of AuCu in M_1 was about 160 times that in D_1 and D_2 ,

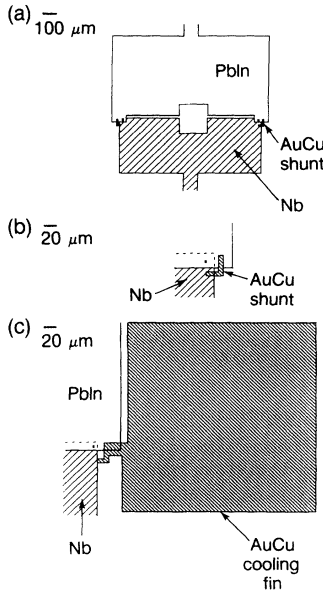


FIG. 11. Configuration of dc SQUIDs, (a) For $D1$ and $D2$ with detail of shunt shown in (b), (c) detail of shunt and cooling fin for $M1$ and $M2$.

and the volume in $M2$ about 30 times that in $M1$.

We measured the noise using the circuit of Fig. 6 with each SQUID, in turn, substituted for the resistor R in the upper chamber of Fig. 7; in the case of $M2$, we used a measuring SQUID with a 50-turn input coil. In this configuration, since $R \ll R_0$, the measured SQUID is essentially voltage biased; variations in flux Φ in the SQUID produce changes in the current I passing through the SQUID. Thus the measuring SQUID detects changes in the current passing through the measured SQUID. We passed a current (filtered at 4.2 K) through an additional coil coupled to the SQUID to provide an appropriate flux bias. The SQUID was biased at a flux $\Phi \approx (m \pm \frac{1}{4})\Phi_0$ (m is an integer) where the transfer function $dI/d\Phi$ is close to a maximum. We adjusted the bias current I until the white noise was a minimum: typically this occurred close to the bias point that maximized the transfer coefficient. We measured the noise generated by the SQUID over the bandwidth 16–20 kHz where the excess low-frequency noise was relatively small (typically the excess low-frequency noise from the SQUID in this frequency range was about equal to the white noise from the SQUID at the lowest temperatures). This frequency range was well below the roll-off frequency of the input circuit, typically ≈ 50 kHz. We subtracted out the noise of the measuring SQUID and its electronics, which we

determined by turning off the bias current in the test SQUID and subtracting the Lorentzian power spectrum produced by Nyquist noise in R_0 from the measured noise power. When the test SQUID was biased at the operating point, the noise from R_0 was negligible. We used a least-squares analysis to fit the measured noise power spectrum of the test SQUID to the functional form $[S_I(f) + A/f^\alpha]$, where $S_I(f)$ is the spectral density of the white-noise current from the SQUID and A and α are constants. From $S_I(f)$ we computed $\varepsilon_v(f) = S_I(f)/2L(dI/d\Phi)^2$ using the measured values of $dI/d\Phi$.

B. Results for SQUIDs with small shunts

Figure 12 shows measured values of ε_v vs bath temperature for SQUID's $D1$ and $D2$. As the temperature is lowered from 4.2 K, ε_v scales with T_0 as expected from Eq. (5.1). Below about 150 mK, however, the noise energy abruptly flattens out as T_0 is further reduced. For SQUID $D2$ at a bath temperature of 22 mK, the noise energy was about $14\hbar$, corresponding to an effective temperature of about 150 mK. This noise energy is substantially higher than the value of about $2.2\hbar$ predicted from the extrapolation of the data above 150 mK (see Table I). Similar results are listed for SQUID $D1$.

The flattening of ε_v as the temperature is lowered occurs at a much higher value than that predicted for quantum-mechanical effects,³³ so this can be ruled out as a mechanism. An alternative possible mechanism by which ε_v could flatten as T_0 is lowered is the existence of an external noise source, for example, in the biasing flux or current. Such a source would be independent of T_0 and uncorrelated with the intrinsic SQUID noise. In this case, ε_v would have the functional form

$$\varepsilon_v = a_0 + b_0 T_0, \quad (5.2)$$

where a_0 and b_0 are temperature-independent coefficients. The dashed line in Fig. 12 shows the behavior predicted by Eq. (5.2), where we have obtained a_0 and b_0 from the high- and low-temperature asymptotic behavior of the data, respectively. We see that Eq. (5.2) predicts a smooth crossover between the high- and low-temperature regimes that is distinctly different from the abrupt crossover of the data.

Although the data are inconsistent with both quantum effects and external noise, they are entirely consistent with the hot-electron effect. In this case, T_e is given by Eq. (2.13). In Fig. 12, we have also plotted the predicted dependence of ε_v vs T_0 using the measured values of P and Ω and the value of Σ determined in Sec. IV, together

TABLE I. Parameters of four dc SQUIDs.

Device	Ω (μm^3)	A (μm^2)	V (μV)	I (μA)	P (pW)	P/Ω (W m^{-3})	P/A (W m^{-2})	T_{\min} (mK)	ε (\hbar)
$D1$	29	960	1.1	5.0	5.4	1.9×10^5	5.6×10^{-3}	151	13 ± 2
$D2$	29	960	1.1	3.5	3.8	1.3×10^5	4.0×10^{-3}	140	13 ± 2
$M1$	4.6×10^3	0.15×10^6	1.2	4.5	5.4	1.2×10^3	3.5×10^{-5}	55	5 ± 1
$M2$	140×10^3	0.15×10^6	4.0	5.0	20.0	1.4×10^2	1.3×10^{-4}	36	5 ± 1

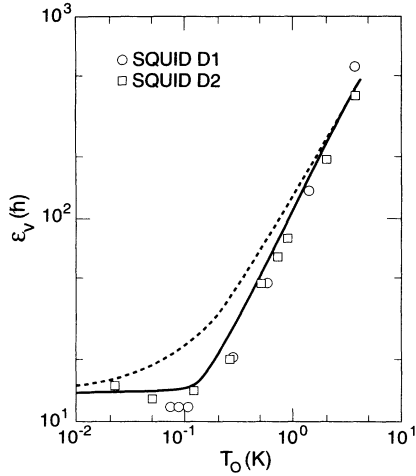


FIG. 12. Flux-noise energy ε_v vs bath temperature T_0 for SQUIDs *D1* and *D2*. The solid line is the prediction of Eq. (5.1) with T given by Eq. (2.13). The dashed line is the prediction of Eq. (5.2).

with Eq. (5.1). The agreement of the prediction with the data is excellent, given that we have used no fitting parameters. Our estimates of $T_{\min} = (P/\Sigma\Omega)^{1/5}$ are listed in Table I for SQUIDs *D1* and *D2*, together with the values obtained by direct measurement. The predictions and measured values of T_{\min} are also in good agreement. We conclude that the noise energy of the two SQUIDs at low temperatures was limited by hot electrons in the shunt resistors.

C. Results for SQUIDs with cooling fins

We turn now to the results from SQUIDs *M1* and *M2* which had large cooling fins attached to the shunt resistors. We chose the configurations of the fins to have a negligible effect on the resistance of the shunts while providing a large volume into which hot electrons could diffuse. The measured values of the intrinsic energy sensitivity ε_v for these two SQUIDs are plotted in Fig. 13, together with the data from SQUIDs *D1* and *D2*. The scatter in the data at low temperatures is higher than at high temperatures because the excess low-frequency noise in the SQUIDs and the noise in the measuring system make a relatively larger contribution. The solid line in Fig. 13 is from the theoretical prediction given by Eq. (5.2), with the SQUID inductance $L=0.5$ nH, SQUID resistance $R=6$ Ω , and $T=T_0$ the bath temperature. We see that the noise energy for the type-*M* SQUIDs begins to flatten off at about 70 mK, falling to about $4\hbar$ at the lowest temperatures. The low-temperature values of ε_v for the *M*-SQUIDs correspond to effective temperatures of 50 ± 10 mK which are consistent with our estimates from $(P/\Sigma\Omega)^{1/5}$ (see Table I). We note that the measured values of ε_v tend to fall somewhat as T_0 is lowered from 60 to 20 mK. This may be due to the increase in the electronic inelastic diffusion length (about 2.5 mm at 50 mK) as T_0 is lowered, thereby causing the effective volume of the fins to increase slightly.

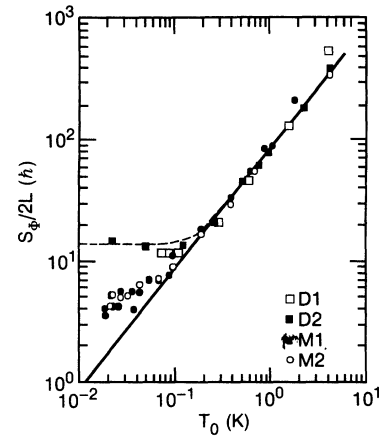


FIG. 13. Flux-noise energy ε_v vs bath temperature T_0 for four SQUIDs. The solid line is the prediction of Eq. (5.2) with $T_e=T_0$, the dashed line is the prediction of Eq. (5.1) for SQUIDs *D1* and *D2* with T_e given by Eq. (2.13).

We note that the limiting noise energy of SQUID *M2* was not significantly better than that of SQUID *M1*, despite the fact that Ω was larger by a factor of 30, and thus one might have expected T_{\min} to be lower by a factor of about 2. However, the electron temperature is determined by the power per unit volume, so that a 30-fold increase in volume reduces the temperature by a factor of 2 provided that the power is the same. In fact, we were forced to operate device *M2* at a higher bias current, and thus at a higher power, than the other devices (see Table I) because there was resonant structure on the I - V characteristic at low temperatures. This structure is associated with microwave resonances in the SQUID circuit and leads to substantial increases in noise if the device is operated on this region of the I - V characteristic. The structure tends to be enhanced as β_c is increased; the value of β_c for SQUID *M2* was somewhat higher than usual, about 0.3. As a result, the value of P/Ω for SQUID *M2* was only a factor of 9 lower than for *M1*, and we predict T_{\min} to be smaller by a factor of only 1.5. Given the scatter in the low-temperature data in Fig. 13, this factor is not significant.

We conclude that the addition of large cooling fins to the resistive shunts of our SQUIDs enable us to improve the noise energy by a factor of about 3 at the lowest bath temperatures, about 20 mK. In both configurations, the noise was limited by hot-electron effects in the shunt resistors. We note that it is difficult to increase the effective area of the cooling fins further since their width is already comparable with the thermal diffusion length. In any case, given that T_e scales as $\Omega^{-1/5}$, an order of magnitude increase in linear dimension, from 0.4 to 4 mm, would reduce T_e by a factor of only 2.5. On the other hand, it is realistic to try to improve the performance somewhat by using thicker fins: had we been able to operate SQUID *M2* (with 900-nm-thick fins) at the more typical power of 5 rather than 20 pW, the estimated value of $T_e = (P/\Sigma\Omega)^{1/5}$ would have been about 27 mK, and the noise energy about $2\hbar$.

VI. CONCLUDING REMARKS

We have shown that when power P is uniformly dissipated in a thin metal film at low temperatures, the temperature of the electron gas increases to $T_e = (P/\Sigma\Omega + T_p^5)^{1/5}$. From measurements on AuCu thin films we deduced $\Sigma = (2.4 \pm 0.6) \times 10^9 \text{ W m}^{-3} \text{ K}^{-5}$, an order of magnitude larger than the value estimated from α^* and γ , about $10^8 \text{ W m}^{-3} \text{ K}^{-5}$. An extension of the theory to take into account departures from the free-electron model and to include transverse phonons and umklapp scattering might well resolve or at least reduce this discrepancy. When we attached a cooling fin to the resistor the increase in T_e for a given power dissipation in the resistor was greatly reduced, and T_e scaled approximately as $P^{1/2.7}$, in qualitative agreement with a simple effective-area model. However, it is clear that a more detailed theory for the case of nonuniform dissipation—for example, taking into account electron cooling via electron-electron collision—is very much needed. In our experiments on dc SQUIDs, we showed that dissipation in the shunt resistors caused the electron temperature to level off at about 150 mK, a value that was remarkably well predicted from our earlier measurements on thin films. We were able to reduce this temperature and thus improve the flux noise energy by a factor of about 3 by incorporating cooling fins into our SQUIDs.

These hot-electron effects have significant implications for metallic, thin-film devices at low temperatures, particularly as the dimensions are reduced. We have already seen that the performance of dc SQUIDs can be seriously limited by hot electrons. Thus, to achieve improvements in performance by lowering the temperature below about 0.1 K, one should design the device to operate at the

lowest possible power—a criterion not hitherto discussed in the optimization of SQUIDs.²⁹ Furthermore, one should provide metal heat sinks with the largest possible volume to minimize the electron temperature in the shunts in which the power is dissipated. It should also be noted that the energy sensitivity of a SQUID may level off at a low temperature because of electron heating, thus masking any manifestation of quantum noise.

Hot-electron effects are also to be expected in other normal-metal devices at low temperatures, for example, single-electron transistors and other Coulomb-blockade devices,^{34–37} and may well impose constraints on their performance. Although the power dissipation in these devices is generally quite low, of order 1 pW, we emphasize that it is the power per unit volume which is important. The small size of many of these structures and the weak dependence of the temperature on the power virtually ensure that the electron heating will be significant. Also, we expect heating effects to be substantial in ultrathin films, where the volume-to-surface ratio is small. We hope that the ideas presented in this paper will provide some guidance in the design of thin-metal-film devices intended for operation at millikelvin temperatures.

ACKNOWLEDGMENTS

We would like to acknowledge a number of particularly enlightening conversations with John Martinis, John Price, Dan Rokhsar, and Michael Roukes. This work was supported by the Director, Office of Energy Research, Office of Basic Energy Sciences, Materials Sciences Division of the U.S. Department of Energy under Contract No. DE-AC03-76SF00098.

*Present address: Center for Superconductivity Research, Department of Physics, University of Maryland, College Park, MD 20742-4111.

†Present address: Departamento de Física, University of Chile, Santiago, Chile.

¹J. M. Ziman, *Principles of the Theory of Solids* (Cambridge University Press, Cambridge, 1979).

²W. A. Little, *Can. J. Phys.* **37**, 334 (1959).

³S. I. Anisimov, B. L. Kapeliovich, and T. L. Perel'man, *Sov. Phys. JETP*, **39**, 375 (1975).

⁴G. L. Eesley, *Phys. Rev. Lett.* **51**, 2140 (1983).

⁵G. L. Eesley, *Phys. Rev. B* **33**, 2144 (1986).

⁶J. G. Fujimoto, J. M. Liu, E. P. Ippen, and N. Bloembergen, *Phys. Rev. Lett.* **53**, 1837 (1984).

⁷H. E. Elsayed-Ali, T. B. Norris, M. A. Pessot, and G. A. Mourou, *Phys. Rev. Lett.* **58**, 1212 (1987).

⁸See, for example, S. M. Sze, *Physics of Semiconductors* (Wiley Interscience, New York, 1981).

⁹P. Roubeau, D. Le Fur, and E. J. A. Varoquaux, in *Proceedings of the Third International Cryogenics Engineering Conference*, edited by Scripta Technica Ltd. (Iliffe Scientific and Technical Publications, Guildford, 1970), p. 315.

¹⁰J. C. Wheatley, R. E. Rapp, and R. T. Johnson, *J. Low Temp.*

Phys. **4**, (1971).

¹¹A. C. Anderson and R. E. Peterson, *Phys. Lett.* **38A**, 519 (1972).

¹²M. R. Arai, *Appl. Phys. Lett.* **42**, 906 (1983).

¹³M. L. Roukes, M. R. Freeman, R. S. Germain, R. C. Richardson, and M. B. Ketchen, *Phys. Rev. Lett.* **55**, 422 (1985).

¹⁴P. W. Anderson, E. Abrahams, and T. V. Ramakrishnan, *Phys. Rev. Lett.* **43**, 719 (1979).

¹⁵F. C. Wellstood, C. Urbina, and J. Clarke, *Appl. Phys. Lett.* **54**, 2599 (1989).

¹⁶F. C. Wellstood, Ph.D. thesis, University of California, Berkeley, 1988.

¹⁷J. Liu, T. L. Meisenheimer, and N. Giordano, *Phys. Rev. B* **40**, 7527 (1989).

¹⁸V. F. Gantmakher, *Rep. Prog. Phys.* **37**, 317 (1974).

¹⁹D. Nowak, *Phys. Rev. B* **6**, 3691 (1972).

²⁰V. F. Gantmakher and V. A. Gasparov, *Sov. Phys. JETP* **37**, 864 (1973).

²¹V. A. Gasparov, *Sov. Phys. JETP* **41**, 1129 (1976).

²²A. Schmid, *Z. Phys.* **259**, 421 (1973).

²³B. Keck and A. Schmid, *J. Low Temp. Phys.* **24**, 611 (1976).

²⁴D. Belitz and S. Das Sarma, *Phys. Rev. B* **36**, 7701 (1987), and references therein.

- ²⁵M. R. Halse, Proc. R. Soc. London **265**, 507 (1969).
- ²⁶See Fig. 9.11 in O. V. Lounasmaa, *Experimental Principles and Techniques Below 1K* (Academic, New York, 1974), p. 226.
- ²⁷A. F. Andreev, Zh. Eksp. Teor. Fiz. **46**, 182 (1964) [Sov. Phys. JETP **19**, 1228 (1964)].
- ²⁸P. G. de Gennes, Rev. Mod. Phys. **36**, 225 (1964); *Superconductivity of Metals and Alloys* (Benjamin, New York, 1966), p. 232.
- ²⁹See, for example, J. Clarke, Proc. IEEE **77**, 1208 (1989).
- ³⁰F. C. Wellstood, C. Urbina, and J. Clarke, Appl. Phys. Lett. **50**, 772 (1987).
- ³¹C. D. Tesche and J. Clarke, J. Low Temp. Phys. **29**, 301 (1977); and corrections in J. J. P. Bruines, V. J. De Waal, and J. E. Mooij, J. Low Temp. Phys. **46**, 301 (1982).
- ³²V. J. de Waal, P. Schrijner, and R. Llurba, J. Low Temp. Phys. **54**, 215 (1984).
- ³³R. H. Koch, D. J. Van Harlingen, and J. Clarke, Appl. Phys. Lett. **38**, 380 (1981).
- ³⁴D. V. Averin and K. K. Likharev, J. Low Temp. Phys. **62**, 345 (1986).
- ³⁵T. A. Fulton and D. J. Dolan, Phys. Rev. Lett. **59**, 807 (1987).
- ³⁶L. J. Geerligs, V. F. Anderegg, P. A. M. Holweg, J. E. Mooij, H. Pothier, D. Esteve, C. Urbina, and M. H. Devoret, Phys. Rev. Lett. **64**, 2691 (1990).
- ³⁷H. Pothier, P. Lafarge, P. F. Orfila, C. Urbina, D. Esteve, and M. H. Devoret, Physica B **169**, 573 (1991).

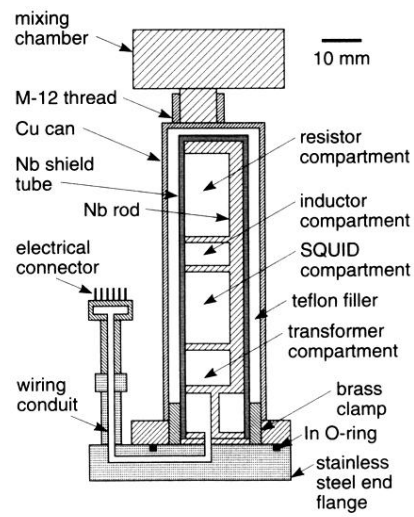


FIG. 7. Experimental cell.